Chapter

Low-Key Stationary and Mobile Tools for Probing the Atmospheric UHI Effect

Kristen Koch, Gunnar W. Schade, Anthony M. Filippi, Garrison Goessler and Burak Güneralp

Abstract

The urban heat island (UHI) effect is created by a series of man-made surface modifications in urban areas that cause changes to the surface energy balance, resulting in higher urban surface air temperatures as compared with surrounding rural areas. Studying the UHI effect is highly amenable to hands-on undergraduate student research projects, because, among other reasons, there are low key measurement tools that allow accurate and regular stationary and mobile probing of air temperature. Here, we summarize the results of a student project at Texas A&M University that analyzed the atmospheric UHI of Bryan/College Station, a mid-size metro area in east Texas. Sling psychrometers were used for semi-regular twice daily stationary air temperature monitoring, and a low-cost electronic sensor and miniature data logger were used for mobile measurements. Stationary data from two similar, open mid-rise building locations showed typical UHI intensities of 0–2°C, while the mobile measurements identified situations with UHI intensities exceeding 6°C when traversing areas with high impervious surface fractions. Nighttime measurements showed the expected UHI intensity relations to wind speed and atmospheric pressure, while daytime data were more strongly related to urban morphology. The success of this research may encourage similar student projects that deliver baseline data to urban communities seeking to mitigate the UHI.

Keywords: sling psychrometer, student project, UHI intensity, mobile measurements, impervious area fraction

1. Introduction

The urban heat island (UHI) effect is a relatively well-researched surface meteorological phenomenon. It describes the difference in surface air temperature between a built-up urban area and its surrounding countryside. Said difference is usually displaying a warmer surface layer air temperature in urban areas, especially during nighttime. Several reviews of the UHI effect magnitudes, characteristics, causes and mitigation strategies can be found in the literature [1–7]. Arnfield [1] summarized the major aspects, stating that UHI intensity is highest at night, typically increases with lower wind speeds under clear sky, high pressure conditions, and is usually more pronounced during summer time and in larger, more populous cities. Recent critique and recommendations for ongoing research [7, 8] have led to

a more streamlined approach of interpreting UHI intensity on the basis of measurement techniques, locations, and urban morphological characterizations such as impervious area fractions, building heights, and canyon aspect ratios.

The causes of UHI effects are related to fundamental differences in the surface energy balance between urban and rural areas. The 3D structure of, and man-made materials in, urban areas cause albedo changes during daytime and "radiation trapping" at night [6, 9–13], causing stronger heat admission during daytime, and slower radiative heat losses at night. In addition, anthropogenic heat from the human population and its energy use in urban areas significantly enhances the UHI effect [14–22]. While rural areas convert a substantial fraction of daytime incoming net radiation into latent heat fluxes, the dominance of impervious areas and an associated lower vegetation density in urban areas compared with their rural surroundings causes a redistribution of incoming net radiation into urban heat storage and sensible heat fluxes. Increased sensible heat fluxes increase the daytime UHI intensity, while high heat storage fluxes exacerbate nighttime UHI intensities when stored heat is returned into the atmosphere [23–28]. Detailed numerical studies such as by Ryu and Baik [29] have shown that impervious surface area, a proxy for energy balance flux changes, is likely the dominant factor determining daytime UHI intensity, while anthropogenic heat releases may dominate nighttime UHI intensity. Both these factors interact with the 3D structure of the urban fabric and the prevailing meteorological conditions. This can cause daytime cool islands as man-made (impervious) surfaces store heat and can shade road "canyons"; and maximum nighttime heat islands as stored heat together with anthropogenic heat are released back into shallower nighttime surface air layers. The results also concur with higher net radiation levels under high pressure conditions in summer, and the associated lack of turbulent heat transport under low wind speeds in urban areas as summarized by Arnfield [1].

To investigate these phenomena, researchers have used both stationary and mobile air temperature measurements extensively. While early studies often used only a few weather station locations [30, 31], or limited mobile traverses [32–34], newer studies have profited from now widely available, small form factor, accurate, and cost-effective electronic temperature sensors deployed in either stationary or mobile fashion. However, the correct deployment and interpretation of such sensors and their data still requires careful consideration, such as of radiation shielding and sensor response time aspects. In comparison, a hand-operated sling psychrometer provides a highly accurate, battery-independent low-key tool that can be operated by any lay person and can be immediately ready at the required time. Sling psychrometers provide dry-bulb and wet-bulb temperatures, and thus serve to provide both air temperature and humidity. They have been used in the past for UHI "spot" measurements [35–37], supplementing weather station and mobile data, and are ideally suited as "hands-on" data collection tools in undergraduate student research projects [38].

This chapter describes a semester-long student project to determine the UHI intensity of a mid-size metropolitan area in east Texas, the Bryan/College Station (BCS) metro area, home of Texas A&M University. As part of a spring semester course on environmental atmospheric science, students were tasked to maintain regular air temperature measurements near the places they lived in town, then turn in a writing assignment at the end of the semester. During the following summer and fall semesters, the first author maintained two of the measurement sites and also carried out a mobile measurement study using her private automobile. Here, we discuss selected results from the measurements in context of past UHI studies. We also introduce an ongoing project of integrating these measurement results with remotely sensed land cover data.

2. Methods

2.1 Sling psychrometer measurements

Sling psychrometers are traditional meteorological measurement tools to determine air temperature (dry-bulb temperature) and relative humidity (wet-bulb temperature). Sling psychrometers have been used in UHI studies going back several decades [32, 35, 36, 39]. They have an educational advantage over automated measurements as they require direct student involvement in the data gathering and documentation process. The instrument used in this study was a Bacharach model 0012-7012 using two red spirit filled glass thermometers with Fahrenheit scales. The instrument is made of a robust hard plastic shell, with its outer part acting as handle when extended, while the inner part bears the two identical glass thermometers. The thermometer scales allow readings as precise as 0.5°F, and are accurate to at least 1.0°F based on intercomparisons with other sling psychrometers and a research grade meteorological sensor, comparisons that were made part of the student project in this UHI study.

Here, we discuss only the dry bulb, aka air temperature data. The atmospheric UHI effect was calculated as the difference between the measured air temperature and the corresponding temperature at 2 m above ground level (agl) at the Texas A&M weather station (**Figure 1**). The weather station's combined T/RH sensor, a

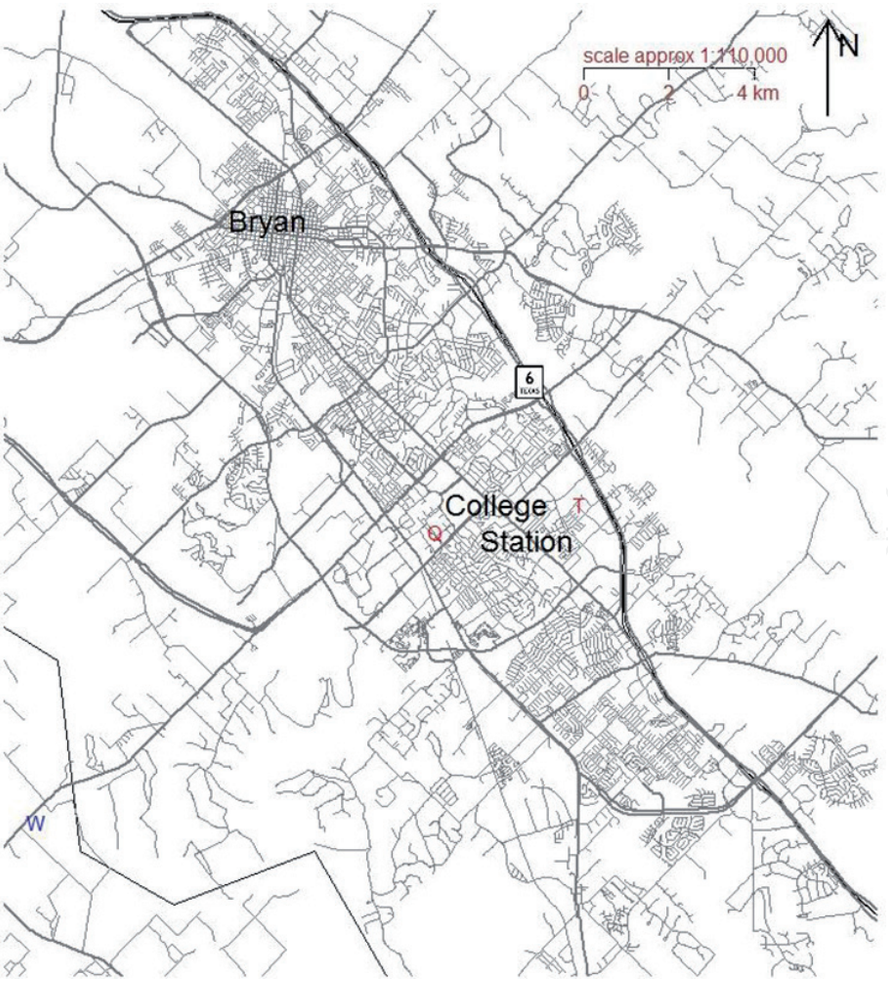

Figure 1.
Roadmap based view of the Bryan/College Station metro area in East Texas (30.6°N, 96.32 W). The major highway traversing the area, Texas-6, is labeled alongside the two stationary measurement locations in red (T = 'trails', Q = 'quad') and the weather station location (W) in blue.

model 085 from MetOne Instruments Inc., has a high precision and accuracy multi-element thermistor (±0.15°C). Corrections for elevation differences between the measurement sites and the weather station reference location were made using the dry adiabatic lapse rate.

Multiple locations were monitored within the BCS metro area during the spring semester of 2015, but only two urban locations, which were monitored throughout 2015, are discussed here. The first location, subsequently identified as the "Trails" apartment complex, was a parking lot area in front of apartment buildings (**Figure 1**) in College Station. This part of town is slightly elevated from the surrounding urban area, and located between a narrow, wooded green corridor, and a major freeway (State Highway 6). While the location was next to pervious lawns, the area was almost tree-less and dominated by buildings, roads, and parking lots. The tallest buildings are the three story apartment buildings; the larger area within half a kilometer, however, includes a midsize mall and associated parking lots to the north, commercial buildings, including hotels, along the freeway to the east, and both taller and less tall apartment buildings toward the south and west.

The second location, subsequently referred to as "Quad", was a small parking lot on the Texas A&M campus in College Station (**Figure 1**). This location is also dominated by impervious surface areas, such as more extensive parking lots to the southeast, large parking garages to the east, and the onsite multi-story dormitories and Dining Hall. It has, however, numerous trees lining the nearby streets. The surroundings within half a kilometer consist of numerous, multi-story university buildings to the north and west, an open park, a field, and a wooded, one-story residential neighborhood to the southwest and south, and a golf course further to the northeast.

Both locations can be characterized as local climate zones (LCZ) 5_6, open mid-rise to low-rise urban areas with 30–50% impervious area [8]. However, Trails is located closer to the east end of town, with rural areas (LCZ B/C) as close as 1.5 km to the east, while Quad is located more central to the metro area, with open, sparsely build-up LCZ 9 areas more than 2 km distant, and rural areas more than 4 km distant (**Figure 1**).

UHI intensity was determined for each location by comparing observed local temperatures to the rural temperature measurement (10-min average) at Texas A&M's weather station 10 km outside the urban area toward the southwest. In addition, we assembled weather station data (pressure, winds, solar radiation, and precipitation) for the days measurements were taken for data analysis.

2.2 Mobile measurements

Air temperature sensors and associated logging equipment have become both miniaturized and highly affordable, thus allowing both high spatial density distributed and low-key mobile data collection of the urban heat island [40]. Mobile measurements (traverses) using automobiles, but also bicycle-mounted or personally carried sensors, have been used numerous times in the past to study the UHI effect, both in long- and in short-term campaigns [32, 33, 37, 41–65].

In summer and fall 2015, we carried out an undergraduate student research project [38] using a standard HOBO U12 data logger with 12-bit temperature sensor (model TMC6-HD) from Onset Computer Inc. to evaluate the atmospheric urban heat island of the BCS metro area. The sensor has a typical accuracy of ±0.25°C and is recorded at a better than 0.2°C resolution. It was placed into a passive radiation shield (model RS3, Onset Comp. Inc.), which was mounted to an angular steel bracket attached to a metal sleeve with a flat rubber sheet that slides over a passenger car side window (**Figure 2**). With the window moved nearly all the way up, the

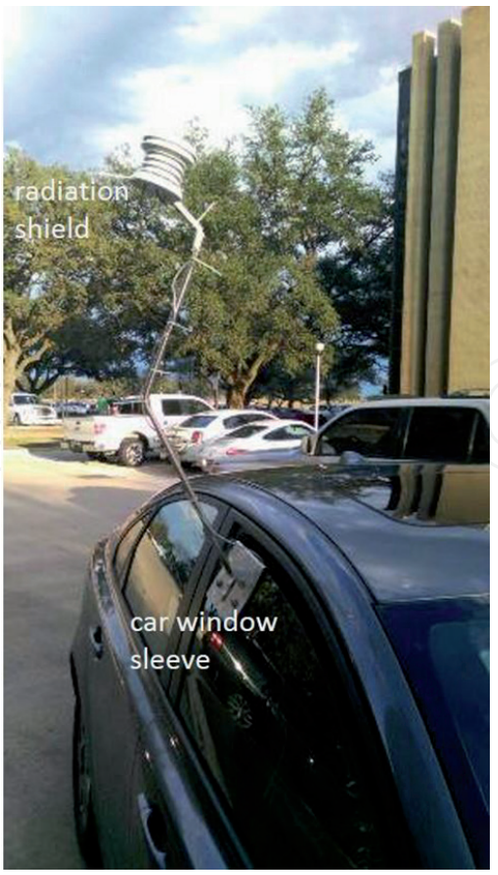

Figure 2.
Mobile measurement setup.

sensor was measuring air temperature at approximately 2 m agl off the passenger side of the car, with its logger safely placed inside the air-conditioned vehicle. This avoided most temperature bias effects from the vehicle itself, or from other vehicles on the road, unless measurements occurred either at very low speeds with air moving across the front hood of the car toward the sensor, such as may have occurred when stopping at traffic lights; or when hot exhaust plumes from vehicles on the road were encountered. Such possible temperature measurement biases, though occasionally encountered, were not removed from the data set.

Typical car moving speeds were 20–30 mph in town and up 50 mph outside the urban areas (approximately 10–25 m s^{-1}) during all mobile measurements. A smart phone app called RAAH (https://www.raah.co) was used to record the vehicle's location. Data logger and smart-phone times were aligned before each drive. During each traverse data were recorded every 10 s, providing for a typical horizontal resolution of 100+ m. However, considering the sensor's response time, and the accuracy and timing of the location determination, both the absolute bias and uncertainty of a recorded temperature's location were likely larger than 100 m. Such aspects should be considered in all mobile studies when moving speeds are comparable or faster than sensor response times.

Raw temperature data were normalized first for the presumed linear temperature change, if present, during the typically one-hour drive for data collection, then adjusted for elevation differences along the route using the dry adiabatic lapse rate. Both corrections were always significantly smaller than the encountered temperature differences between the rural and (sub-)urban areas traversed.

The routes driven were selected to avoid selective coverage of the metro area, and such that measurements along a route could be completed within approximately 1 h, including nearby rural areas. All routes were driven once in the

morning, and then at least two times during the afternoon and around midnight. Based on student availability during the project, completing the set of selected routes lasted from late August to early November 2015.

One route, which was driven twice during the project, brought the vehicle close to the Texas A&M weather station in the rural area approximately 10 km outside the urban area to the southwest (**Figure 1**). Good agreement between the vehicle based sensor and the weather station sensor was observed (<0.5°C differences), and minimum temperatures during each drive were strongly correlated with weather station temperature during the drive hour (slope = 0.98, $r^2 > 0.99$). Consequently, we used calculated temperature anomalies during each traverse and determined UHI intensity from each drive's observed maximum minus minimum temperature. The remaining meteorological parameters were assembled in similar fashion as described above for the stationary measurements.

2.3 Urban area characterization using remote sensing

To aid in the interpretation of the observed atmospheric UHI effect, we estimated the spatial extent and configuration of various land-cover/land-use (LCLU) areas in Bryan/College Station (BCS), Texas. To this end, we jointly analyzed airborne digital orthophotographs and a LiDAR-derived digital surface model (DSM) of the study area. We thus characterized urban LCLU based on a remote-sensing approach. In particular, we employed a geospatial object-based image analysis (GEOBIA) method [66, 67], which effectively exploits contextual/spatial information. GEOBIA-based image-processing algorithms and data fusion are needed to more fully exploit image information, particularly in the case of high-spatial-resolution data. For our GEOBIA analysis, we employed eCognition® Developer software, which allows objects/segments to be delineated and used to classify geospatial datasets. We divided the processing steps into two phases: an initial remote-sensing data segmentation and classification phase, and a subsequent post-segmentation/classification editing phase, which we conducted to improve classification accuracy. We performed quantitative classification accuracy assessment on the revised, post-classification edited result.

2.3.1 Segmentation and classification phase

Data sets and data pre-processing. Data processing for this remote-sensing segmentation/classification analysis began with the acquisition of multiple 50-cm natural-color (NC)/color-infrared (CIR) Digital Orthophoto Quarter Quad (DOQQ) images, acquired from the Texas Natural Resource Information System (TNRIS). These images were collected between October 2014 and August 2015 as part of the 2015 Texas Orthoimagery Program. We mosaicked the DOQQs for the BCS, Texas study area, and then spatially resampled the mosaic to a 5-m grid cell size in order to facilitate subsequent completion of GEOBIA computational processing. Additionally, we utilized a high-point-density LiDAR point cloud, acquired from Texas A&M University, which was collected in conjunction with the State of Texas over the February 9–10, 2015 period. We filtered and processed the LiDAR point cloud using Esri ArcGIS LAS tools to produce a digital surface model (DSM) of the BCS area. After initial processing of the image and LiDAR data, we spatially subset the respective data sets using a polygon to fit the same areal extents.

Information classes and training set delineation. The LCLU information classes employed in this analysis are: roads, roofs, other impervious, trees, lawns, water, bare soil, and pasture/cropland. The pasture/cropland class is actually a combined pasture/grassland/cropland class, which contains grasslands that are not (residential)

Class ID number	Class name	Number of training polygons
1	Roads	62
2	Roofs	281
3	Other Impervious	43
4	Trees	43
5	Lawns	153
6	Water	219
7	Bare Soil	39
8	Pasture/Cropland	46

Table 1.
Number of training polygons per class, used for GEOBIA-based LCLU classification of Bryan/College Station (BCS), Texas study area.

lawns. We manually delineated the training areas based on manual/visual interpretation of the aerial photography and DSM. We initially generated training areas for a set of 15 classes, then later merged some of these classes, yielding the aforementioned final set of eight information classes. The distribution of training-area polygons across these classes is given in **Table 1**.

GEOBIA parameter values, input variables, and ruleset development. We created a ruleset within eCognition® Developer using the imagery, DSM, and training areas. The process involved multiple steps, including: segmentation, class assignment using the training areas, assigning the classified segments as samples, configuring the nearest-neighbor classifier, and applying/conducting the classification. We determined GEOBIA parameter values via iterative, trial-and-error experimentation, with the objective of maximizing LCLU map classification accuracy, while also accounting for computational constraints of the GEOBIA system/computing environment. For the classification step, we used a nearest-neighbor classification algorithm. The classification input features included: mean blue band, mean green band, mean red band, mean near-infrared (NIR) band, mean DSM, standard deviation blue band, standard deviation green band, standard deviation red band, standard deviation NIR band, standard deviation DSM, normalized difference vegetation index (NDVI) [68], and normalized difference water index (NDWI) [69]. We applied the classifier at the image-object level [66], and exported classification results in both vector and raster formats, where we subjected the latter product (at 5-m cell size) to subsequent processing and analysis.

2.3.2 Post-segmentation/classification editing phase

The resultant LCLU classification entailed various areas of clear misclassifications, including some roads, parking lots, and roofs/buildings. Therefore, we performed some post-/segmentation/classification editing to increase classification accuracy of the class information. In particular, publicly available geographic information system (GIS) data from the City of College Station and the Brazos County Appraisal District aided editing of the LCLU classification map. For roads, we used a vector GIS layer containing road center lines, where we buffered the center lines, 5 m on each side, followed by a dissolve operation. We assigned the road classification value to the buffered area, converted to the data to the raster data model, and then overwrote the pixels in the original LCLU map in these areas with these road classification values. For the roofs class, we followed a similar procedure, except that no buffers were used. Since we only had access to building

footprint data from the City of College Station, we only applied this operation to areas within College Station, and not the City of Bryan; however, a large portion of the study area lies within the City of College Station boundary. For the other impervious class, based on visual interpretation of the aerial photography, we digitized impervious areas—especially parking lots—where misclassifications were evident. After rasterization of the digitized polygons, we then overwrote misclassified pixels in the original LCLU raster using these newly digitized data. Based on visual inspection, these post-classification GIS operations generally markedly improved classification accuracy. One caveat though is that although the DOQQs and LiDAR point clouds were collected close in time, the data in the vector GIS layers used in this post-segmentation/classification editing phase were acquired some time prior to the DOQQ and LiDAR acquisitions, and this temporal disjunction may have resulted in some errors in the edited LCLU map, particularly given the relatively high rate of urbanization in the BCS area in recent years. Furthermore, future analysis may entail using variable buffer distances for the road centerlines, depending upon road type.

2.3.3 Quantitative land-cover/land-use classification accuracy assessment

Using standard methods [70, 71], we performed a quantitative thematic/classification accuracy assessment on the finalized land-cover/land-use (LCLU) classified map, edited post-classification. We employed a stratified random sampling approach for generating the classification accuracy-assessment points/sample locations, and we used 100 such points per class [70, 71]. We used the DOQQ aerial photograph mosaic as the reference data; we evaluated the accuracy of the post-classification-edited LCLU map via manual/visual interpretation of the DOQQs at the stratified random point locations. This analysis enabled the generation of an error matrix from which we computed statistics, including the overall accuracy [72, 73]. The overall classification accuracy of the post-classification edited LCLU map was 76.5%.

3. Results and discussion

3.1 Stationary measurements

Stationary measurements were commenced past the semester-long student project to evaluate whether there was a seasonality to the UHI in BCS. As shown in **Figure 3**, no clear seasonal variation was observed. However, the five highest UHI intensities, all above 4°C, were all measured during spring-time (March and April). They occurred on clear or mostly clear-sky days after recent cold front passages, and possible reasons for high values under those conditions are discussed below. Lowest values, down to −1.3°C, indicative of a local urban cool island, occurred dominantly during morning measurements. Comparing sites and measurement times, the median morning UHI intensity was slightly, but statistically significantly lower than the median night/evening UHI intensity. Site differences were statistically insignificant.

Figure 4 shows that the UHI intensity was slightly dependent on large-scale wind directions. Northerly winds, as occur behind cold front passages, were responsible for the spring-time maxima in UHI intensity at the Trails site, but no such significant difference could be found for the Quad site. This could be due to the fact that a mid-size mall, a 0.4 km^2 large area of impervious surface area, lies just beyond a narrow green corridor north of the Trails site, but no such prominent heat source lies near the Quad site.

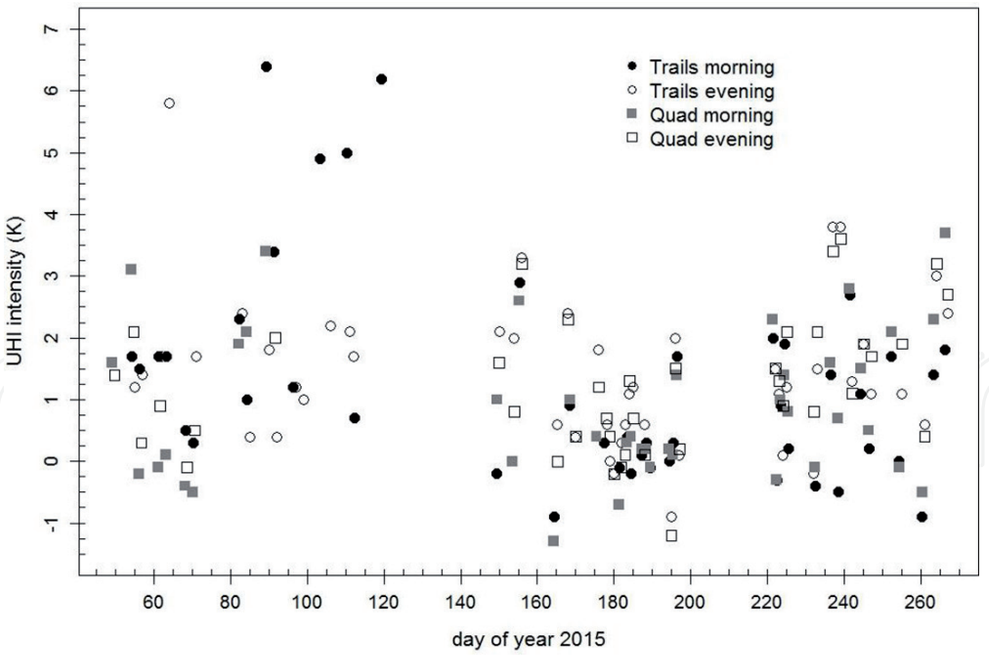

Figure 3.
Seasonal changes of UHI intensity for the stationary sites and measurement times in 2015.

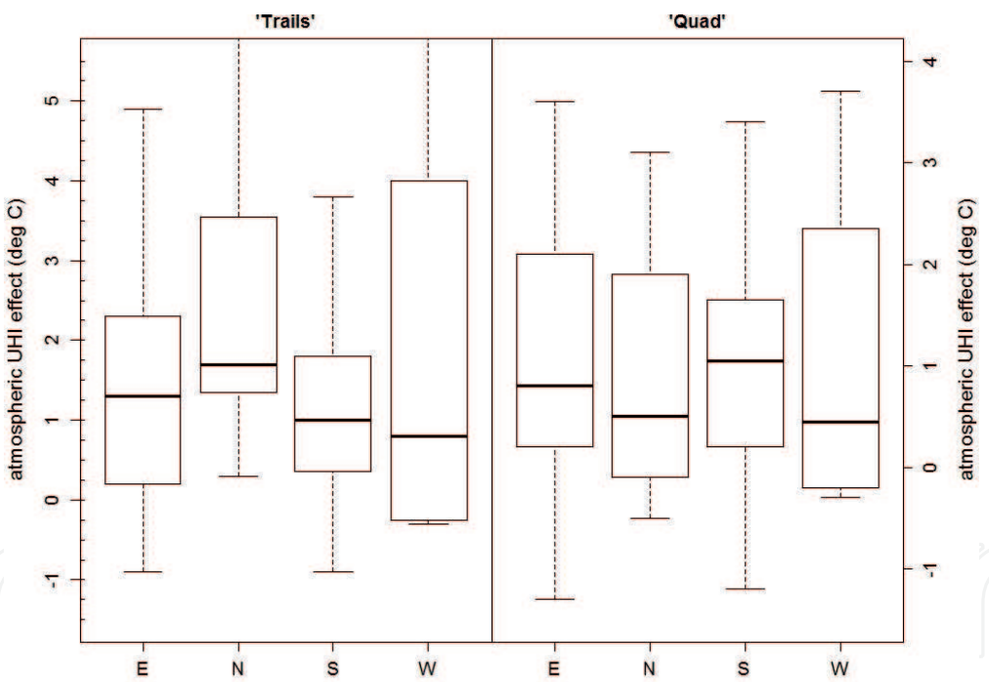

Figure 4.
Boxplot of all 2015 UHI intensity measurements as a function of cardinal wind direction during the observation period. Thick horizontal bars mark medians, box edges mark the interquartile range (IQR), and whiskers are 95% confidence interval estimates.

We used a multi-linear regression to evaluate whether and which meteorological factors may have contributed to the UHI intensity at each site. Eliminating wind direction, we found that lower temperature, and lower relative humidity days were significantly ($p > 0.95$) correlated with the UHI intensity, a result strongly driven by the high spring values though. In addition, days with higher pressures were significantly correlated with the observed UHI intensity at the Quad site ($p > 0.95$). However, no statistically significant relationship with (rural) wind speed, ranging from 0 to 7 m s^{-1}, was found. In summary, no single meteorological parameter other than wind direction (**Figure 4**) stood out in explaining the observations.

The observed UHI intensity range is comparable with similar measurements in other mid-size urban areas (e.g. [33, 39, 74]). However, parameters other than population (or city) size and meteorological conditions are typically more relevant, particularly impervious area fraction, anthropogenic heat release, and urban morphology [29]. Therefore, we can surmise that because both our sites have a higher than average canyon aspect ratio (building height, *H*, to canyon width, *W*, ratio), and higher than average population and thus energy use density, morning cool island findings could be related to shading and strong heat admittance into the urban fabric [75–77], while the highest UHI intensities may have been related to high local anthropogenic heat emissions, respectively. This will be discussed in more detail with respect to LCZ classifications elsewhere.

3.2 Mobile measurements

The selected driving routes covered central areas north and south of the city border between Bryan and College Station, where impervious surface areas maximize (LCZ 3 and 5). They also covered residential areas in south College Station, where LCZ 6 dominates.

Figure 5 shows an overview of results from three representative late evening drives, depicting three of the four routes. These drives occurred on (from north to south) September 16, August 28, and October 14, 2015. Rural wind directions and speeds for those drives were SE at 3–4 m s^{-1}, ESE at 1–2 m s^{-1}, and ESE at 3–4 m s^{-1}, respectively.

In total, 15 traverses were completed at night and 16 during daytime (12 afternoon and 4 mornings). The nighttime traverses showed UHI intensities of 3.2 ± 1.9 K (mean + − 1 sd), while the daytime UHI intensities were lower at

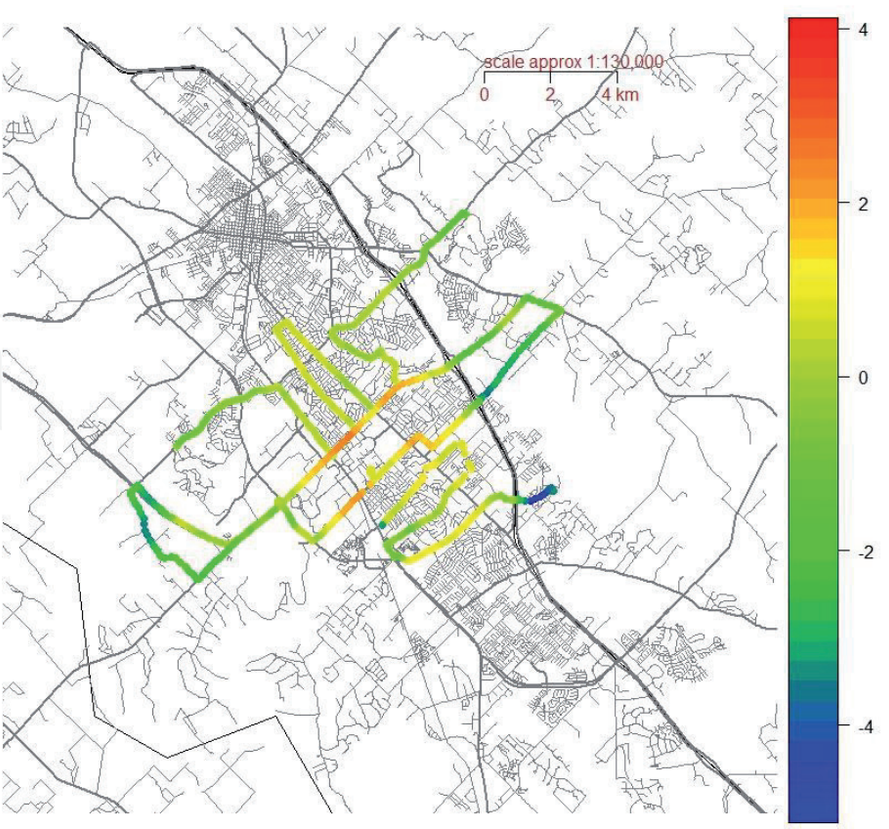

Figure 5.
Roadmap based view of the BCS urban metro area overlaid with temperature anomalies (in Kelvin) during three representative late evening traverses. All traverses occurred under weak southeasterly winds. The central traverse on August 26, 2015 had the lowest wind speeds and a UHI intensity of 6.1 K.

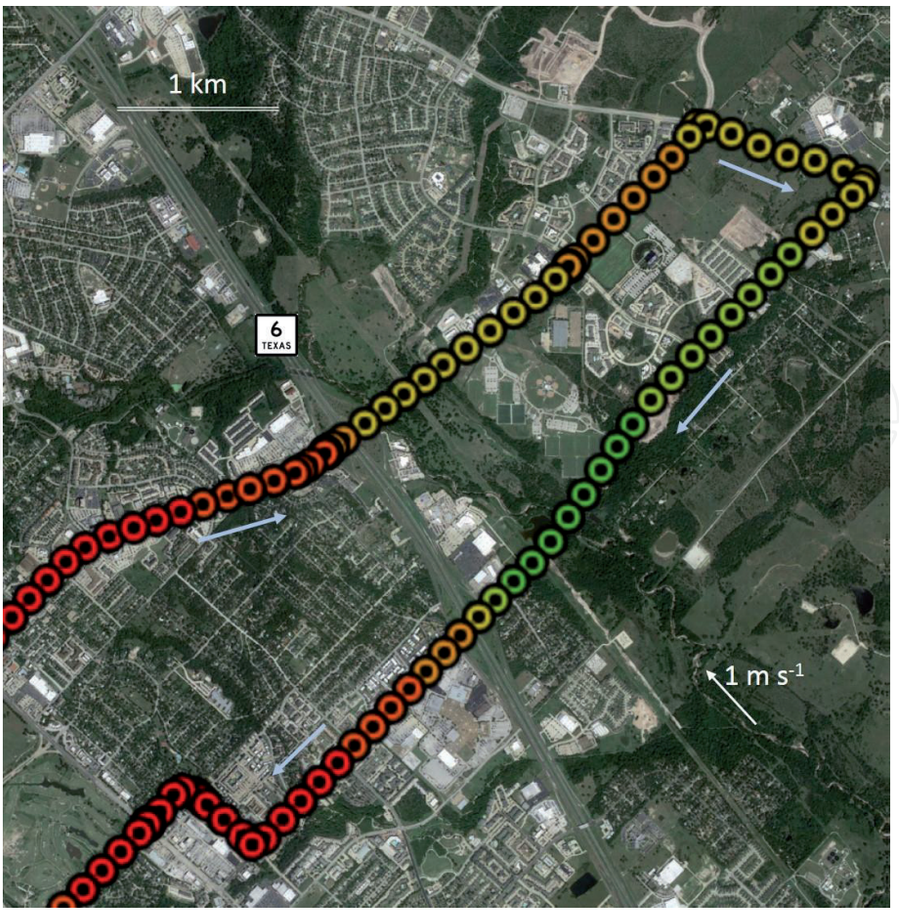

Figure 6.
Sectional GE overlay of mobile air temperature measurements during the late evening traverse on August 26, 2015. The white arrow shows wind speed and direction during the traverse. Driving direction is indicated by the light blue arrows, and relative driving speed can be deduced from symbol spacing. Symbols designate temperatures ranging from 29.5° C (red) in the road sections downwind densely build-up urban areas 1–2 km to the west of highway 6, to 26° C (yellow) downwind the irrigated outdoor sports complex near the center of the map, to 24° C (green) downwind of the then (2015) undeveloped area southeast of the sports complex.

2.3 ± 1.2 K. Only the nighttime UHI intensities displayed clear relationships to the prevailing meteorological conditions, namely atmospheric pressure and wind speed ($p > 0.99$), but also air temperature itself ($p > 0.95$). In addition, a weak dependence on the day's solar radiation totals was observed ($p > 0.77$). The daytime traverses' UHI intensities were not significantly related to the meteorological data; only air temperature ($p > 0.87$) and solar radiation ($p > 0.78$) were weakly related to UHI intensity for the afternoon traverses.

The combined data maintained dependencies on wind speed ($p > 0.95$) and atmospheric pressure ($p > 0.9$), and, together with the above, these results indicate that the UHI intensity of this midsize urban area was significantly more pronounced at night- as compared with daytime conditions. The day-night difference, as well as the relationships with wind speed, atmospheric pressure, and related cloud cover, reproduced findings from previous UHI studies [1].

The results from the mobile measurements will be used further to analyze the major urban drivers of UHI intensity in terms of LCZ type [8, 52, 57, 63, 78–84], and associated impervious area fractions and aspect ratios [29, 85–87].

Here, we show two case studies: one using a typical Google Earth (GE) view, and one using remotely sensed urban land cover. **Figure 6** shows a GE view of a part of the eastern BCS urban area, where the local highway separated a densely build-up area from a large outdoor sports facility, featuring frequent lawn irrigation and open, mostly undeveloped land to its southeast.

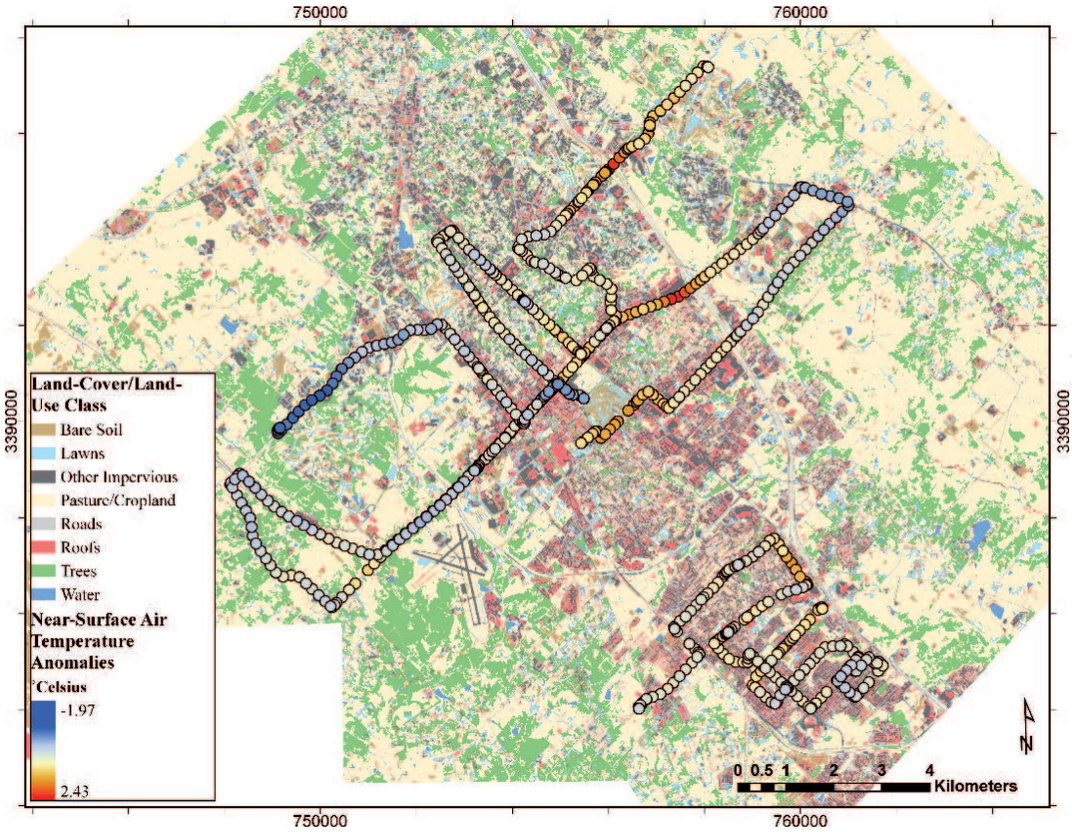

Figure 7.
Temperature anomalies from several daytime (afternoon) traverses, overlaid on the LCLU map of the BCS area. The depicted routes were driven on September 2, 2015 (central SW–NE extension; winds E at 4 m s^{-1}), October 14, 2015 (southern extension; winds SE at 4 m s^{-1}), and August 26, 2015 (northern extension; winds S at 3.5 m s^{-1}). X and y-axis units are in meters and reflect easting *and* northing *of UTM zone R14 (i.e., distance, respectively, from the central meridian of the zone and from the equator).*

Temperatures dropped 3°C crossing the highway toward the east into a less developed area, and another 2°C once downwind of a largely undeveloped area at the time (LCZ B/C/D). Driving direction and symbol spacing highlighted in this close-up illustrate the delayed response of the temperature sensor at higher driving speeds on the southern leg as compared with the northern leg, which included two short stops at traffic lights, one before crossing the highway, and another north of the sports complex near the center of the map.

Case study 2 is shown in **Figure 7**, which depicts temperature anomalies from three independent daytime traverses overlaid on the high resolution LCLU map. The daytime traverses showed a much more sophisticated, smaller scale pattern of the UHI as compared with the nighttime traverses. Wind speed during all these drives was south to southeasterly, and upon closer inspection the data revealed impacts of impervious surfaces areas near and upwind of the driving location [38, 88] as an important factor in determining UHI intensity in the BCS metro area. Research is ongoing to improve the LCLU map, and quantify UHI intensity as a function of the footprint's impervious area fraction, as well as other LCZ properties such as canyon aspect ratio and surface albedo.

4. Conclusions

We have translated an undergraduate course project of stationary measurements of the urban heat island in a mid-size urban area in east Texas into a more detailed undergraduate study of the cities' UHI intensity as a function of meteorological conditions and urban morphology. Our study was able to reproduce the

expected UHI intensity relationships with wind speed and atmospheric pressure, emphasizing synoptic high pressure conditions with intense solar radiation as a major driver of the UHI. In addition, we may have also found effects of local anthropogenic heat release and building shading. The latter, urban morphology and its local to regional impacts, is an ongoing focus of UHI research. We find that not only on larger scales is the UHI effect advected downwind, but local temperatures during daytime are advected downwind on a sub-kilometer scale [8]. Hence, the fraction of impervious area immediately upwind may more strongly affect local air temperature than the local impervious area fraction at the point of measurement. Future work is intended to better quantify this effect for the urban area studied. If confirmed, and of significant size, this opens avenues for local area UHI effect mitigation planning. It suggests that previous calls for (i) more surface unsealing to reduce urban runoff and increase surface moisture and (ii) increased tree cover for additional shading and latent heat cooling, may indeed be the two most efficient pathways to reduce the UHI locally, at least in mid-size metropolitan areas, where LCZs 5 and 6 dominate.

Acknowledgements

We are grateful to the College of Geosciences, Texas A&M University, for funding the two undergraduate students involved in this project.

Author details

Kristen Koch[1], Gunnar W. Schade[2*], Anthony M. Filippi[3,4], Garrison Goessler[3,4] and Burak Güneralp[3,4]

1 Environmental Programs, Texas A&M University, College Station, USA

2 Department of Atmospheric Sciences, Texas A&M University, College Station, USA

3 Department of Geography, Texas A&M University, College Station, USA

4 Center for Geospatial Sciences, Applications and Technology (GEOSAT), Texas A&M University, College Station, USA

*Address all correspondence to: gws@geos.tamu.edu

References

[1] Arnfield AJ. Two decades of urban climate research: A review of turbulence, exchanges of energy and water, and the urban heat island. International Journal of Climatology. 2003;**23**(1):1-26

[2] Mohajerani A, Bakaric J, Jeffrey-Bailey T. The urban heat island effect, its causes, and mitigation, with reference to the thermal properties of asphalt concrete. Journal of Environmental Management. 2017;**197**:522-538

[3] Akbari H, Kolokotsa D. Three decades of urban heat islands and mitigation technologies research. Energy and Buildings. 2016;**133**:834-842

[4] Tzavali A, Paravantis JP, Mihalakakou G, Fotiadi A, Stigka E. Urban heat island intensity: A literature review. Fresenius Environmental Bulletin. 2015;**24**(12B):4535-4554

[5] Lee JS, Kim JT, Lee MG. Mitigation of urban heat island effect and greenroofs. Indoor and Built Environment. 2014;**23**(1):62-69

[6] Gago EJ, Roldan J, Pacheco-Torres R, Ordonez J. The city and urban heat islands: A review of strategies to mitigate adverse effects. Renewable & Sustainable Energy Reviews. 2013;**25**:749-758

[7] Stewart ID. A systematic review and scientific critique of methodology in modern urban heat island literature. International Journal of Climatology. 2011;**31**(2):200-217

[8] Stewart ID, Oke TR. Local climate zones for urban temperature studies. Bulletin of the American Meteorological Society. 2012;**93**(12):1879-1900

[9] Zhou DC, Zhao SQ, Liu SG, Zhang LX, Zhu C. Surface urban heat island in China's 32 major cities: Spatial patterns and drivers. Remote Sensing of Environment. 2014;**152**:51-61

[10] Kakoniti A, Georgiou G, Marakkos K, Kumar P, Neophytou MKA. The role of materials selection in the urban heat island effect in dry mid-latitude climates. Environmental Fluid Mechanics. 2016;**16**(2):347-371

[11] Morini E, Touchaei AG, Castellani B, Rossi F, Cotana F. The impact of albedo increase to mitigate the urban Heat Island in Terni (Italy) using the WRF model. Sustainability. 2016;**8**(10):999

[12] Wang YP, Akbari H. Analysis of urban heat island phenomenon and mitigation solutions evaluation for Montreal. Sustainable Cities and Society. 2016;**26**:438-446

[13] Arnfield AJ, Grimmond CSB. An urban canyon energy budget model and its application to urban storage heat flux modeling. Energy and Buildings. 1998;**27**(1):61-68

[14] Salamanca F, Martilli A, Yague C. A numerical study of the urban Heat Island over Madrid during the DESIREX (2008) campaign with WRF and an evaluation of simple mitigation strategies. International Journal of Climatology. 2012;**32**(15):2372-2386

[15] Ichinose T, Shimodozono K, Hanaki K. Impact of anthropogenic heat on urban climate in Tokyo. Atmospheric Environment. 1999;**33**(24-25):3897-3909

[16] Hinkel KM, Nelson FE, Klene AF, Bell JH. The urban heat island in winter at Barrow, Alaska. International Journal of Climatology. 2003;**23**(15):1889-1905

[17] Kim Y-H, Baik J-J. Spatial and temporal structure of the urban Heat

Island in Seoul. Journal of Applied Meteorology. 2005;**44**(5):591-605

[18] Hinkel KM, Nelson FE. Anthropogenic heat island at Barrow, Alaska, during winter: 2001-2005. Journal of Geophysical Research-Atmospheres. 2007;**112**(D06118). DOI: 10.1029/2006JD007837

[19] Lee SH, McKeen SA, Sailor DJ. A regression approach for estimation of anthropogenic heat flux based on a bottom-up air pollutant emission database. Atmospheric Environment. 2014;**95**:629-633

[20] Boehme P, Berger M, Massier T. Estimating the building based energy consumption as an anthropogenic contribution to urban heat islands. Sustainable Cities and Society. 2015;**19**:373-384

[21] Chapman S, Watson JEM, McAlpine CA. Large seasonal and diurnal anthropogenic heat flux across four Australian cities. Journal of Southern Hemisphere Earth Systems Science. 2016;**66**(3):342-360

[22] Zhou DC, Zhang LX, Hao L, et al. Spatiotemporal trends of urban heat island effect along the urban development intensity gradient in China. Science of the Total Environment. 2016;**544**:617-626

[23] Park C, Schade GW, Werner ND, Sailor DJ, Kim CH. Comparative estimates of anthropogenic heat emission in relation to surface energy balance of a subtropical urban neighborhood. Atmospheric Environment. 2016;**126**:182-191

[24] Vesala T, Jarvi L, Launiainen S, et al. Surface-atmosphere interactions over complex urban terrain in Helsinki, Finland. Tellus B. 2008;**60**(2):188-199

[25] Jarvi L, Grimmond CSB, Taka M, et al. Development of the surface urban energy and water balance scheme (SUEWS) for cold climate cities. Geoscientific Model Development. 2014;**7**(4):1691-1711

[26] Ao XY, Grimmond CSB, Chang YY, et al. Heat, water and carbon exchanges in the tall megacity of Shanghai: Challenges and results. International Journal of Climatology. 2016;**36**(14):4608-4624

[27] Loridan T, Lindberg F, Jorba O, et al. High resolution simulation of the variability of surface energy balance fluxes across Central London with urban zones for energy partitioning. Boundary-Layer Meteorology. 2013;**147**(3):493-523

[28] Ward HC, Kotthaus S, Jarvi L, Grimmond CSB. Surface urban energy and water balance scheme (SUEWS): Development and evaluation at two UK sites. Urban Climate. 2016;**18**:1-32

[29] Ryu YH, Baik JJ. Quantitative analysis of factors contributing to urban Heat Island intensity. Journal of Applied Meteorology and Climatology. 2012;**51**(5):842-854

[30] Holmer B, Eliasson I. Urban-rural vapour pressure differences and their role in the development of urban heat islands. International Journal of Climatology. 1999;**19**(9):989-1009

[31] Runnalls KE, Oke TR. Dynamics and controls of the near-surface heat island of Vancouver, British Columbia. Physical Geography. 2000;**21**(4):283-304

[32] Goldreich Y. Urban climate studies in Johannesburg, a Suptropical City located on a ridge - a review. Atmospheric Environment Part B-Urban Atmosphere. 1992;**26**(3):407-420

[33] Park H-S. Features of the heat island in Seoul and its surrounding cities. Atmospheric Environment (1967). 1986;**20**(10):1859-1866

[34] Saitoh TS, Shimada T, Hoshi H. Modeling and simulation of the Tokyo urban heat island. Atmospheric Environment. 1996;**30**(20):3431-3442

[35] Akinbode OM, Eludoyin AO, Fashae OA. Temperature and relative humidity distributions in a medium-size administrative town in Southwest Nigeria. Journal of Environmental Management. 2008;**87**(1):95-105

[36] Tso CP. A survey of urban heat island studies in two tropical cities. Atmospheric Environment. 1996;**30**(3):507-519

[37] Deosthali V. Impact of rapid urban growth on heat and moisture islands in Pune City, India. Atmospheric Environment. 2000;**34**(17):2745-2754

[38] Comrie AC. Mapping a wind-modified urban heat island in Tucson, Arizona (with comments on integrating research and undergraduate learning). Bulletin of the American Meteorological Society. 2000;**81**(10):2417-2431

[39] Yamashita S, Sekine K, Shoda M, Yamashita K, Hara Y. On relationships between heat island and sky view factor in the cities of Tama River basin, Japan. Atmospheric Environment (1967). 1986;**20**(4):681-686

[40] Honjo T, Yamato H, Mikami T, Grimmond CSB. Network optimization for enhanced resilience of urban heat island measurements. Sustainable Cities and Society. 2015;**19**:319-330

[41] Kuttler W, Barlag AB, Rossmann F. Study of the thermal structure of a town in a narrow valley. Atmospheric Environment. 1996;**30**(3):365-378

[42] Spronken-Smith RA, Oke TR. The thermal regime of urban parks in two cities with different summer climates. International Journal of Remote Sensing. 1998;**19**(11):2085-2104

[43] Upmanis H, Eliasson I, Lindqvist S. The influence of green areas on nocturnal temperatures in a high latitude city (Goteborg, Sweden). International Journal of Climatology. 1998;**18**(6):681-700

[44] Torok SJ, Morris CJG, Skinner C, Plummer N. Urban heat island features of southeast Australian towns. Australian Meteorological Magazine. 2001;**50**(1):1-13

[45] Unger J, Sumeghy Z, Zoboki J. Temperature cross-section features in an urban area. Atmospheric Research. 2001;**58**(2):117-127

[46] Jonsson P. Vegetation as an urban climate control in the subtropical city of Gaborone, Botswana. International Journal of Climatology. 2004;**24**(10):1307-1322

[47] Huang LM, Zhao DH, Wang JZ, Zhu JY, Li JL. Scale impacts of land cover and vegetation corridors on urban thermal behavior in Nanjing, China. Theoretical and Applied Climatology. 2008;**94**(3-4):241-257

[48] Sun CY, Brazel AJ, Chow WTL, Hedquist BC, Prashad L. Desert heat island study in winter by mobile transect and remote sensing techniques. Theoretical and Applied Climatology. 2009;**98**(3-4):323-335

[49] Yokobori T, Ohta S. Effect of land cover on air temperatures involved in the development of an intra-urban heat island. Climate Research. 2009;**39**(1):61-73

[50] da Silva VDR, de Azevedo PV, Brito RS, Campos J. Evaluating the urban climate of a typically tropical city of northeastern Brazil. Environmental Monitoring and Assessment. 2010;**161**(1-4):45-59

[51] Charabi Y, Bakhit A. Assessment of the canopy urban heat island of a

coastal arid tropical city: The case of Muscat, Oman. Atmospheric Research. 2011;**101**(1-2):215-227

[52] Alexander PJ, Mills G. Local climate classification and Dublin's urban Heat Island. Atmosphere. 2014;**5**(4):755-774

[53] Borbora J, Das AK. Summertime urban Heat Island study for Guwahati City, India. Sustainable Cities and Society. 2014;**11**:61-66

[54] Busato F, Lazzarin RM, Noro M. Three years of study of the urban Heat Island in Padua: Experimental results. Sustainable Cities and Society. 2014;**10**:251-258

[55] Szegedi S, Toth T, Lazar I. Role of urban morphology in development of the thermal excess in the City of Debrecen, Hungary. Environmental Engineering and Management Journal. 2014;**13**(11):2805-2808

[56] Dobrovolny P, Krahula L. The spatial variability of air temperature and nocturnal urban heat island intensity in the city of Brno, Czech Republic. Moravian Geographical Reports. 2015;**23**(3):8-16

[57] Leconte F, Bouyer J, Claverie R, Petrissans M. Using local climate zone scheme for UHI assessment: Evaluation of the method using mobile measurements. Building and Environment. 2015;**83**:39-49

[58] Czubaszek R, Wysocka-Czubaszek A. Urban Heat Island in Bialystok. Journal of Ecological Engineering. 2016;**17**(3):60-65

[59] Qaid A, Bin Lamit H, Ossen DR, Shahminan RNR. Urban heat island and thermal comfort conditions at micro-climate scale in a tropical planned city. Energy and Buildings. 2016;**133**:577-595

[60] Chakraborty T, Sarangi C, Tripathi SN. Understanding Diurnality and inter-seasonality of a sub-tropical urban Heat Island. Boundary-Layer Meteorology. 2017;**163**(2):287-309

[61] Liu L, Lin YY, Liu J, et al. Analysis of local-scale urban heat island characteristics using an integrated method of mobile measurement and GIS-based spatial interpolation. Building and Environment. 2017;**117**:191-207

[62] Dihkan M, Karsli F, Guneroglu N, Guneroglu A. Evaluation of urban heat island effect in Turkey. Arabian Journal of Geosciences. 2018;**11**(8):186. Available from: https://doi.org/10.1007/s12517-018-3533-3

[63] Shi Y, Lau KKL, Ren C, Ng E. Evaluating the local climate zone classification in high-density heterogeneous urban environment using mobile measurement. Urban Climate. 2018;**25**:167-186

[64] Yadav N, Sharma C. Spatial variations of intra-city urban heat island in megacity Delhi. Sustainable Cities and Society. 2018;**37**:298-306

[65] Ziter CD, Pedersen EJ, Kucharik CJ, TurnerMG.Scale-dependentinteractions between tree canopy cover and impervious surfaces reduce daytime urban heat during summer. Proceedings of the National Academy of Sciences. 2019;**116**(15):7575-7580

[66] Benz UC, Hofmann P, Willhauck G, Lingenfelder I, Heynen M. Multi-resolution, object-oriented fuzzy analysis of remote sensing data for GIS-ready information. ISPRS Journal of Photogrammetry and Remote Sensing. 2004;**58**(3-4):239-258

[67] Blaschke T. Object based image analysis for remote sensing. ISPRS Journal of Photogrammetry and Remote Sensing. 2010;**65**(1):2-16

[68] Rouse JW, Haas RH, Schell JA, Deering DW, Freden SC, Mercanti EP,

et al., editors. Monitoring Vegetation Systems in the Great Plains with ERTS. Greenbelt: NASA; 1974

[69] McFeeters SK. The use of the normalized difference water index (NDWI) in the delineation of open water features. International Journal of Remote Sensing. 1996;**17**(7):1425-1432

[70] Congalton RG. A review of assessing the accuracy of classifications of remotely sensed data. Remote Sensing of Environment. 1991;**37**(1):35-46

[71] Congalton RG, Green K. Assessing the Accuracy of Remotely Sensed Data: Principles and Practices. Bocan Raton: Lewis Publishers; 1999

[72] Filippi AM, Jensen JR. Fuzzy learning vector quantization for hyperspectral coastal vegetation classification. Remote Sensing of Environment. 2006;**100**(4):512-530

[73] Filippi AM, Jensen JR. Effect of continuum removal on hyperspectral coastal vegetation classification using a fuzzy learning vector quantizer. IEEE Transactions on Geoscience and Remote Sensing. 2007;**45**(6):1857-1869

[74] Oke TR. City size and the urban heat island. Atmospheric Environment (1967). 1973;7(8):769-779

[75] Santamouris M. Analyzing the heat island magnitude and characteristics in one hundred Asian and Australian cities and regions. Science of the Total Environment. 2015;**512**:582-598

[76] Alonso MS, Fidalgo MR, Labajo JL. The urban heat island in Salamanca (Spain) and its relationship to meteorological parameters. Climate Research. 2007;**34**(1):39-46

[77] Giovannini L, Zardi D, de Franceschi M. Analysis of the urban thermal fingerprint of the city of Trento in the Alps. Journal of Applied Meteorology and Climatology. 2011;**50**(5):1145-1162

[78] Cai M, Ren C, Xu Y, Dai W, Wang XM. In: Lai PC, Low CT, Wong PPY, editors. International Conference on Geographies of Health and Living in Cities: Making Cities Healthy for all. 2016;**36**(iii-iv):82-89

[79] Cai M, Ren C, Xu Y. 2017 Joint Urban Remote Sensing Event. IEEE; 2017

[80] Cardoso RD, Amorim M. Urban heat island analysis using the 'local climate zone' scheme in Presidente Prudente, Brazil. Investigaciones Geograficas-Spain. 2018;**69**:107-118

[81] Lin ZL, Xu HQ. In: Weng Q, Gamba P, Xian G, Chen JM, Liang S, editors. A study of urban heat island intensity based on local climate zones: A case study in fuzhou, china. 4th International Workshop on Earth Observation and Remote Sensing Applications. Guangzhou, China; 2016:250-254. DOI: 10.1109/EORSA.2016.7552807

[82] Skarbit N, Stewart ID, Unger J, Gal T. Employing an urban meteorological network to monitor air temperature conditions in the 'local climate zones' of Szeged, Hungary. International Journal of Climatology. 2017;**37**:582-596

[83] Wang CY, Middel A, Myint SW, et al. Assessing local climate zones in arid cities: The case of Phoenix, Arizona and Las Vegas, Nevada. ISPRS Journal of Photogrammetry and Remote Sensing. 2018;**141**:59-71

[84] Wang ZH, Xing W, Huang Y, Xie TA. Studying the urban Heat Island using a local climate zone scheme. Polish Journal of Environmental Studies. 2016;**25**(6):2609-2616

[85] Kolokotroni M, Giridharan R. Urban heat island intensity in London: An

investigation of the impact of physical characteristics on changes in outdoor air temperature during summer. Solar Energy. 2008;**82**(11):986-998

[86] Memon RA, Leung DYC, Liu CH. Effects of building aspect ratio and wind speed on air temperatures in urban-like street canyons. Building and Environment. 2010;**45**(1):176-188

[87] Theeuwes NE, Steeneveld GJ, Ronda RJ, et al. Seasonal dependence of the urban heat island on the street canyon aspect ratio. Quarterly Journal of the Royal Meteorological Society. 2014;**140**(684):2197-2210

[88] Heaviside C, Cai XM, Vardoulakis S. The effects of horizontal advection on the urban heat island in Birmingham and the west midlands, United Kingdom during a heatwave. Quarterly Journal of the Royal Meteorological Society. 2015;**141**(689):1429-1441